The effect of building geometry on the size of aeolian deposition patterns
Scale model experiments at the beach

Poppema , Daan W.; Wijnberg, Kathelijne M.; Mulder, Jan P.M. ; Vos, Sander E.; Hulscher, Suzanne J.M.H.

DOI
10.1016/j.coastaleng.2021.103866

Publication date
2021

Document Version
Final published version

Published in
Coastal Engineering

Citation (APA)
Poppema , D. W., Wijnberg, K. M., Mulder, J. P. M., Vos, S. E., & Hulscher, S. J. M. H. (2021). The effect of building geometry on the size of aeolian deposition patterns: Scale model experiments at the beach. *Coastal Engineering*, *168*, 1-16. Article 103866. https://doi.org/10.1016/j.coastaleng.2021.103866

Coastal Engineering 168 (2021) 103866

Contents lists available at ScienceDirect

Coastal Engineering

journal homepage: www.elsevier.com/locate/coastaleng

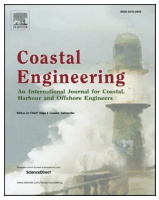

The effect of building geometry on the size of aeolian deposition patterns: Scale model experiments at the beach

Daan W. Poppema [a,*], Kathelijne M. Wijnberg [a], Jan P.M. Mulder [a], Sander E. Vos [b], Suzanne J.M. H. Hulscher [a]

[a] Water Engineering and Management, University of Twente, P.O. Box 217, 7500 AE, Enschede, the Netherlands
[b] Department of Hydraulic Engineering, Delft University of Technology, P.O. Box 5048, 2600 GA, Delft, the Netherlands

ARTICLE INFO

Keywords:
Roughness element
Obstacles to wind flow
Sand drift
Urbanized beach
Structure-from-motion photogrammetry
Characteristic length scale

ABSTRACT

In sandy environments, like the beach-dune system, buildings not only affect the airflow, but also the aeolian sediment transport in their surroundings. In this study, we determine how the horizontal size of sediment deposition patterns around buildings depends on the building's dimensions. Four one-day experiments were conducted at the beach using box-shaped scale models. We tested 32 building geometries, where scale model height, width and length ranged between 0.3 and 2.0 m. The deposition patterns were substantial in size: the total length and width of the deposition area were up to an order of magnitude larger than the horizontal building dimensions. It was found that the size of upwind and downwind deposition patterns depended more on the building width perpendicular to the wind direction (w), than on the building height (h). Building length had little influence. Especially the combined effect of w and h correlated well with horizontal deposition size. This is expressed in a new scaling length B for deposition around buildings, with $B = w^{2/3} \cdot h^{1/3}$. As a first validation, the spatial dimensions of the initial deposition patterns observed around a scale model of $2.5 \times 12 \times 2.5$ m, placed at the beach for five weeks, showed good agreement with those predicted based on B.

1. Introduction

All over the world, people enjoy recreation at the beach. As a result, more and more buildings like restaurants, beach huts and houses are built at the beach-dune interface (see Fig. 1) (Hoonhout and Waagmeester, 2014; Malavasi et al., 2013). However, sandy coasts are vulnerable areas where beaches and dunes represent important natural and recreational values and, especially in low lying countries like the Netherlands, dunes serve as primary flood protection. Buildings affect the wind-driven sand transport in their surroundings and thereby affect the natural development of the very same dunes (Jackson and Nordstrom, 2011). In addition, sediment deposition and erosion around buildings can be a hindrance to building owners and beach visitors.

Buildings at the beach or in the beach-dune interface reduce the source area for windblown sediment transport (García Romero et al., 2016; Morton et al., 1994) and alter the wind field in their surroundings (Jackson and Nordstrom, 2011; Nordstrom and McCluskey, 1984; Smith et al., 2017). In the front and lee of buildings, flow deceleration and reversal can decrease sediment fluxes, leading to sedimentation. Conversely, the deflection of wind around buildings or underneath elevated buildings can create an acceleration zone with increased sediment transport and erosion (Jackson and Nordstrom, 2011; Smith et al., 2017). The sediment transport can be increased further by the higher turbulent intensity of the wind behind buildings (Smith et al., 2017). Furthermore, continuous lines of buildings can also act as a barrier to sand transport and cause fetch segmentation by detaching dunes from their beach or foredune sources (Jackson and Nordstrom, 2011; Smith et al., 2017). As a result of these effects, patterns of erosion and sedimentation arise around buildings.

Buildings in the beach-dune interface cause erosion and sedimentation, so they can steer dune development and affect dune development rates in their surroundings. Smith et al. (2017) and García Romero et al. (2016) found that cities at the Canary Islands have both stabilizing and destabilizing effects on adjacent dune fields. Nordstrom and McCluskey (1984) observed that houses actually built in the dunes can modify the dune form and cause depressions around the houses. Furthermore, the analysis of field measurements and aerial photos of dunes around Dutch beach buildings showed that buildings can have a significant effect on

* Corresponding author.
E-mail address: d.w.poppema@utwente.nl (D.W. Poppema).

https://doi.org/10.1016/j.coastaleng.2021.103866
Received 16 July 2020; Received in revised form 5 February 2021; Accepted 6 February 2021
Available online 9 February 2021

the long-term duneward sand transport (Hoonhout and Van Thiel de Vries, 2013; Reinders et al., 2014).

These morphological effects of buildings near the beach-dune interface can pose a safety risk to buildings themselves but also to hinterlands that depend on dunes for flood protection. Local deposition around buildings temporarily decreases the amount of landward sediment transport that remains available to be blown further into the dunes. In the long term, this can have detrimental effects on dune growth and hence on safety in a larger area. In addition, erosion around buildings can create weak spots in the dune line (Nordstrom and McCluskey, 1984, 1985). Furthermore, at the level of shorter term sediment dynamics, deposition induced by buildings can cause a considerable hindrance to beach users, especially when occurring on beach entrances, walkways and terraces (Jackson and Nordstrom, 2011). Furthermore, natural values can suffer when dune vegetation is affected by changes in the sediment dynamics around buildings (Hoonhout and Van Thiel de Vries, 2013).

The abovementioned effects can pose serious problems to building owners, but also raise challenges for regional authorities and coastal managers who have to balance the interests of recreation, flood safety and nature with regards to permission and regulations for the construction of these buildings (Nordstrom and McCluskey, 1984; Winckel et al., 2008). Therefore, quantitative knowledge is required on the effects of buildings, the spatial extent over which buildings affect their surroundings and how this depends on the building type.

Previous research into the morphological effects of buildings mostly described the erosion and deposition around specific scale models of buildings in a wind tunnel (Iversen et al., 1990; McKenna Neuman and Bédard, 2015; Tominaga et al., 2018). Systematic and quantitative knowledge is lacking on how sedimentation and erosion patterns depend on building design (building size and shape, use of poles to allow airflow under buildings), building location (distance from dune and other buildings) and building orientation (Hoonhout and Van Thiel de Vries, 2013; Hoonhout and Waagmeester, 2014). This knowledge gap hampers knowledge-supported regulations for beach-side buildings and limits capabilities to design and position beach-side buildings in such a way to minimize impact and reduce the hindrance of sedimentation and the need for sediment removal.

As a first step, this research aims to determine how the location and horizontal size of initial aeolian deposition patterns around buildings on the beach depend on the building's dimensions. The dependencies have been determined based on field tests with 32 scale models. By focussing on the initial deposition patterns we highlight the direct effects of buildings before morphologic feedback starts to interact with these patterns. To ensure that deposition patterns can develop without topographic constraints and under uniform wind conditions, buildings are examined on an open beach. Derived relationships have been validated against results of one full-scale model test. Given the lack of knowledge of large-scale effects of buildings on the beach-dune system, this paper focuses on the larger scale deposition patterns around buildings, rather than on the local erosion features directly at the corners of the buildings (Poppema et al., 2019).

In this paper, we first present an overview of the expected effects of building dimensions on airflow and sedimentation patterns based on literature (section 2), followed by a description of the experimental set-up, the data collection and analysis methods (section 3). In section 4 we present the results of the experiments and predictive relationships between building dimensions and size of initial deposition patterns. Finally, the paper ends with a discussion and conclusion.

2. Theory on airflow and sediment dynamics around buildings

Aeolian deposition and erosion patterns around buildings are the direct effect of airflow around buildings. Therefore, existing studies on airflow patterns around buildings (e.g. Hunt, 1971; Martinuzzi and Tropea, 1993; Peterka et al., 1985) can be used to hypothesize how building size and shape quantitatively depend on the size of sedimentation and erosion patterns. However, the step from flow structures to sand transport and to sedimentation and erosion patterns is far from straightforward (Kok et al., 2012), so the effect of building properties on sand transport and morphology have to be studied explicitly.

2.1. Airflow around buildings

The airflow pattern around bluff objects like buildings differs markedly from the airflow over natural bedforms and dunes. In both cases, flow is diverted over and around an object. However, over streamlined bedforms, flow more or less follows the topography, whereas at sharp building edges (additional) flow separation, recirculation and turbulence occur. As a result, the wind around buildings forms a horseshoe vortex and creates a highly turbulent wake behind the building (Fackrell, 1984; Hunt, 1971, Fig. 11 Martinuzzi and Tropea, 1993; Peterka et al., 1985).

The formation of this horseshoe vortex (Fig. 2) can be explained by the wind profile approaching the building. Wind approaching a building causes increased pressure at the upwind building face. Part of the wind is directly diverted over the building and to the sides. However, as wind velocity and thereby pressure increase with elevation, a downward flow is also formed. The upward and downward flows are separated by a stagnation zone at around $^{2}/_{3}$ to ¾ of the building height (Peterka et al., 1985). Above this zone, the wind is diverted upwards and to the sides. Below this zone, the wind is diverted downwards and to the sides. This downward flow creates a reverse flow close to the ground, upwind of the building, which leads to a rotating vortex in front of the building. This vortex is wrapped around the building by the wind, thereby obtaining the horseshoe shape (Hunt, 1971; Martinuzzi and Tropea, 1993; Peterka

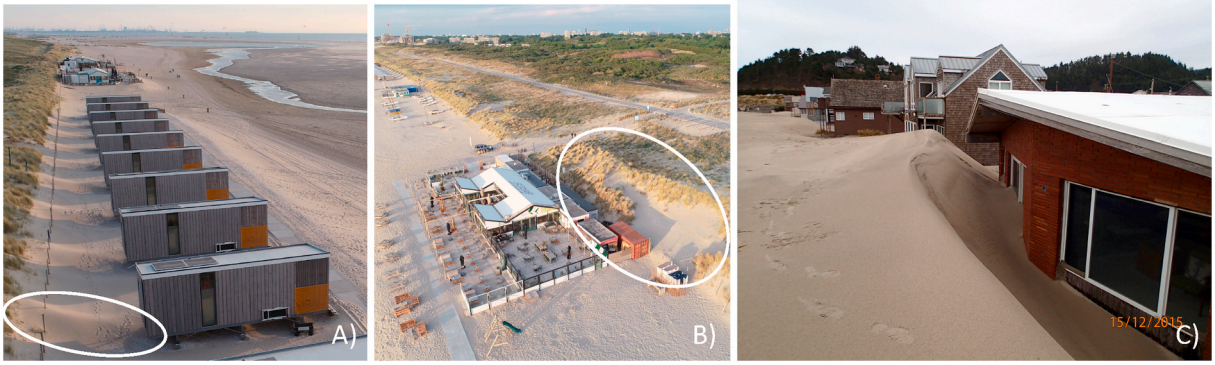

Fig. 1. Buildings on the beach. A) A row of holiday houses with some deposition behind the houses (e.g. the white oval), in Kijkduin, The Netherlands. B) A beach restaurant with a more bare dune behind it (the white oval) in Kijkduin, The Netherlands. C) Houses with substantial deposition built in Pacific City, USA (photo courtesy of Oregon Parks and Recreation Department).

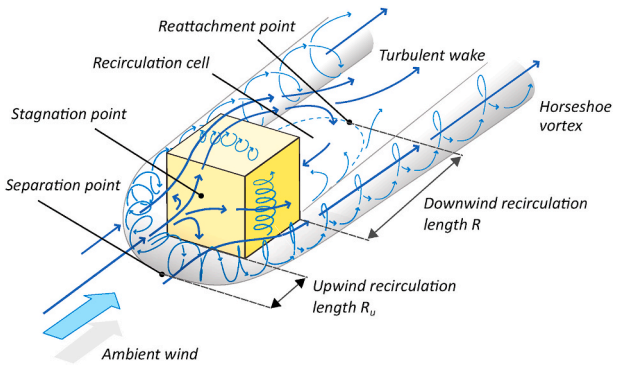

Fig. 2. The airflow patterns around a building oriented perpendicular to the wind (adapted from Oke et al., 2017).

et al., 1985).

The size of the vortex upwind of the building and hence the upwind recirculation length R_u (i.e. the distance between the flow separation point and the upwind building edge) depend on the building width (w) and height (h) (Beranek, 1984; Martinuzzi and Tropea, 1993; Peterka et al., 1985) and on the turbulent intensity (Peterka et al., 1985). With increasing building width or height, more wind is diverted, increasing the vortex size. Beranek (1984) approximated this effect with $R_u = 0.7\sqrt{wh}$ for aspect ratios (w/h ratios) between 0.8 and 3. However, for increasing building width, the effect is partially counteracted by more wind being diverted over the building instead of to the sides, causing a lowering of the stagnation point (Martinuzzi and Tropea, 1993). Consequently, in the experiments of Martinuzzi and Tropea (1993), $R_u = 0.8w^{0.4}h^{0.6}$ matched the results better for similar aspect ratios. Furthermore, they noted that the separation length becomes almost width-independent for wide buildings, between aspect ratios of 4 and 6.

The separated flow over the building edges can reattach at the top and sides of the building. Whether it reattaches before reaching the back of the building depends on the building's length-to-width and length-to height ratio and on the turbulent intensity (Fackrell, 1984; Hunt, 1971; Peterka et al., 1985). This reattachment roughly occurs if building length l is larger than $\frac{1}{2}\sqrt{h}$ (Fackrell, 1984). If flow reattaches on the building, a separate recirculation cell, also called a separation cavity, is formed downwind of the building. If flow reattachment does not occur, the flow at the side and top of the building forms one joint recirculation cell with the flow behind the building (Martinuzzi and Tropea, 1993; Peterka et al., 1985). In this case, the downwind recirculation length, so the distance between the downwind building edge and the flow reattachment point behind the building (see Fig. 2) becomes larger (Fackrell, 1984).

The downwind recirculation length R can be described with eq. (1) (ASHRAE, 2005; Wilson, 1979).

$$R = \min(w,h)^{2/3} \cdot \max(w,h)^{1/3}, 1/8 < w/h < 8 \quad (1)$$

Alternative relationships between building dimensions and recirculation length can be found in e.g. Fackrell (1984) and Martinuzzi and Tropea (1993). Downwind of the recirculation cell, the airflow in the building wake still differs from the undisturbed wind field by having, along the centreline behind the building, a lower mean velocity and a higher turbulent intensity. For building aspect ratios between 1 and 4, this wake extends behind the building up to a distance of 10–30 times the building height (Peterka et al., 1985). Taking x as the distance behind the building, the velocity deficit decays with $x^{-1.3}$ behind approximately cubical buildings (Hunt, 1971; Peterka et al., 1985) and with x^{-1} behind really wide buildings (Hunt, 1971). With wind being diverted to the sides, wind in the horseshoe vortex behind a building (i.e. more to the sides) has both a higher velocity and a higher turbulent intensity.

2.2. Erosion-deposition patterns around buildings

The airflow around buildings affects windblown sediment transport, giving rise to deposition and erosion patterns. Wind tunnel experiments on erosion and deposition around buildings (Iversen et al., 1990, 1991; Tominaga et al., 2018) reported strong erosion at the upwind building edge and especially the upwind corners. Deposition occurred some distance upwind of the building and downwind in the lee of the building, with the latter also being referred to as a shadow dune or sand shadow (Bagnold, 1941; Luo et al., 2012). A phenomenological examination of sand deposition and erosion around our scale models at the beach (Poppema et al., 2019) agreed with the erosion at the upwind building edge and the upwind deposition area a small distance upwind of the building. In addition, strong deposition tails were found downwind of the building and occasionally along the building, approximately at the location of the horseshoe vortex tails in Fig. 2. Similar deposition features were reported in several experiments on snow accumulation around buildings (Liu et al., 2018; Thiis, 2003; Thiis and Gjessing, 1999; see Poppema, 2020 for an overview), that were performed both in wind tunnels and in the field.

The next step is quantitatively linking the size of this deposition to building dimensions. As quantitative knowledge on the location of sedimentation and erosion is poorly developed, related processes can be used to improve understanding of these deposition and erosion patterns. For example, deposition upwind of beach buildings can be compared to echo dunes in front of natural vertical cliffs as found in deserts and at beaches (Tsoar, 1983; Tsoar and Blumberg, 1991). Tsoar (1983) examined echo dune formation upwind of such cliffs using a wind tunnel. He observed that dunes formed a small distance upwind of the cliffs. Using cliff height h and a cliff over the full wind tunnel width, the initial separation distance was 0.3 h–0.4 h, while the dune crest was located at 0.5 h–0.6 h upwind of the cliff. As echo dunes grew higher, their crest remained at the same location, but the edge grew toward the cliff.

The scaling of airflow structures around buildings with building dimensions may be used as a basis to predict the size of deposition patterns. However, airflow and sand transport around buildings are expected to differ in how they depend on building height. Wind speed increases away from the bed. Hence, the amount of wind blocked or diverted by buildings increases more than linearly with building height. Sand transport, to the contrary, is mainly concentrated in a saltation layer close to the bed. Common saltation layer heights are less than 0.5 m (Dong et al., 2003; Rotnicka, 2013), so lower than any building height. Hence, the amount of blocked or diverted sand transport is expected to increase little with building height. The downwind recirculation length R for airflow behind buildings as described in eq. (1) also functions as a general *scaling length* for airflow around buildings (Wilson, 1979). The length and height of the recirculation cells on top of the building and behind the building scale linearly with R (i.e. their size is proportional to R). Likewise, R is used to describe the width of the recirculation cell and of the building wake (see Fig. 2), airflow streamlines and diffusion around buildings (Schulman et al., 2000). Given that R is used as a scaling length for the airflow and diffusion near buildings, it might also serve as a scaling length to predict the size of aeolian deposition.

However, with building height having less effect on sediment transport than on airflow patterns, the scaling length R as used for airflow patterns likely has to be adapted to be applicable for deposition patterns. Therefore, we introduce B, a new scaling length for deposition around buildings (eq. (2)), in which the powers of $^2/_3$ and $^1/_3$ are kept the same as in R, but the building width is consistently given the larger power to reflect its importance for sand transport. We expect that deposition patterns scale better with scaling length B than with R.

$$B = w^{2/3} \cdot h^{1/3} \quad (2)$$

2.3. Development rate of deposition patterns

Airflow patterns around buildings are generally independent of the wind speed, in the sense that the spatial pattern, expressed as a local wind speed U divided by the undisturbed wind speed U_0, does not depend on U_0 (Fackrell, 1984; Peterka et al., 1985). However, this implies that the *absolute* value of the wind speed at a given location will scale linearly with the undisturbed wind speed. This absolute wind speed is important for the creation of deposition patterns, because it determines the aeolian sediment transport capacity. This in turn affects deposition length, as further described below.

For the wind speed in the far wake of the building (downwind of the recirculation cell), there are some general expressions (Kothari et al., 1986; Peterka et al., 1985) for the dependence of U on the distance downwind of the building, x, allowing us to quantify the effect of wind speed on deposition rate. In the horseshoe vortex, which approximately coincides with the main deposition areas (Thiis and Gjessing, 1999), the wind speed is higher than the undisturbed wind speed. The wind speed excess ($\Delta U/U_0$) decays with the distance downwind of the building. This can be described by eq. (3), in which the wind speed excess decays inversely proportional to x^{β} and α is a constant smaller than 1 (Hansen and Cermak, 1975; Peterka et al., 1985). Such a decreasing wind speed would mean a decreasing sediment transport rate, hence explaining the deposition areas behind a building. Assuming that deposition is dominantly determined by downwind gradients in the wind speed (i.e. neglecting the contribution from local changes in the wind direction) and that the sediment transport rate is proportional to the wind speed to the power n, then eq. (4) describes the sediment transport rate Q_s and eq. (5) the deposition rate $\frac{-dQs}{dx}$. For large x (more than a few times the recirculation length R), the deposition rate is then approximately proportional to $\frac{U_0^n}{x^{1+\beta}}$.

$$U = U_0\left(1+\frac{\alpha}{x^{\beta}}\right) \tag{3}$$

$$Q_s \propto U^n = {U_0}^n \cdot \left(1+\frac{\alpha}{x^{\beta}}\right)^n \tag{4}$$

$$-\frac{dQ_s}{dx} \propto U_0^n \cdot \alpha\beta n \cdot \left(1+\frac{\alpha}{x^{\beta}}\right)^{n-1} \cdot \frac{1}{x^{1+\beta}} \tag{5}$$

Eq. (5) shows that the deposition rate increases with wind speed, so deposition patterns around a building will develop faster at higher wind speeds. We can now also quantify how this affects the observed deposition length over a given timespan, if we assume that a certain minimum elevation change is needed to be detectable in the field as deposition (such as during our experiments).

For a given timespan, the minimum elevation change that defines the edge of the deposition pattern will now occur at a distance x where $dh = \frac{dQ}{dx}.dt$ has a certain value. So for this given timespan, the deposition rate at the detectable edge of the deposition pattern is fixed. Hence, at the deposition edge, $\frac{U_0^n}{x^{1+\beta}}$ is a constant, such that with an increase in U_0, the x-coordinate of the deposition edge will increase proportional to $U_0^{n/(1+\beta)}$. In other words, the deposition length that can develop within a given timespan scales with $U_0^{n/(1+\beta)}$.

It is known that the aeolian sediment transport rate scales approximately quadratically with the wind speed (Kok et al., 2012; Ungar and Haff, 1987), so n is approximately 2. Based on a perturbation analysis, Hunt (as cited by Hansen and Cermak, 1975; Kothari et al., 1979) expected the downwind vortex strength and wind speed excess to scale inversely proportional to $\sqrt{x}$ for $x > 5h$, meaning β is likely close to 0.5. This would make the downwind deposition length proportional to $U_0^{1.33}$. However, this value of β is still uncertain. A decay as quick as $x^{-1.3}$, like Peterka et al. (1985) measured for the velocity deficit at the centreline behind a building, is unlikely due to (extra building-induced) turbulence and vortices that convect air with higher velocities down from higher elevations, thereby delaying the wind speed decay (Kothari et al., 1986). An intermediate value of for instance $\beta = 1$ would result in a deposition length that is exactly linear with U_0. This is quite similar to the result of $U_0^{1.33}$, so even though the exact scaling is still unknown, the initial downwind deposition length that can develop within a given timespan scales close to linearly with wind speed.

For deposition sizes other than the downwind length, the effect of wind speed is more difficult to predict. The analysis for the initial downwind deposition length is based on explicit relations for the downwind gradient in windspeed magnitude. Without explicit descriptions of the lateral gradient and the upwind wind field, the effect of wind speed on the downwind deposition width and upwind width and length cannot be quantified. However, the general principle still holds that at higher wind speeds, a similar gradient in the sediment transport rate (i.e. a similar deposition rate) can be reached at a smaller gradient in the wind speed magnitude, so further from the building. Besides, lateral variations in wind speed are probably more local than downwind variations because advection dominantly works in x-direction. If the lateral decay of wind speed disturbances is faster (if β in eq. (5) is larger), then deposition width is less affected by wind speed than deposition length.

3. Methodology

3.1. Set-up experiments at the beach

A field experiment with scale models of buildings at the beach was used to examine aeolian deposition and erosion patterns around beach buildings (see Fig. 3, Fig. 4). The scale models consisted of cuboid stacks of cardboard boxes. To examine the effect that building size and shape have on the size of deposition patterns, the scale models size and shape were varied. The model length, width, and height ranged between 1 and 4 boxes, with individual boxes being 33 × 50 × 35 cm (w x l x h). Boxes were filled with a sandbag to prevent them from being blown away.

The experiment was conducted at the beach instead of in a wind tunnel, to allow testing under natural conditions and at a natural scale. While wind tunnels are commonly used to model airflow around buildings, modelling sediment transport as well is more problematic as it involves the scaling of additional processes (creep, saltation), quantities (grain density, fall velocity, sediment flux) and length and time scales (grain size, saltation layer height, saturation length). Unfortunately, these cannot be properly scaled due to irreconcilable processes and dimensionless numbers (Duthinh and Simiu, 2011; White, 1996). Furthermore, turbulent field conditions are notoriously difficult to simulate in wind tunnels (Duthinh and Simiu, 2011) but indispensable for the flow structures around buildings (Peterka et al., 1985; Smith et al., 2017). By placing models at the beach, the models could be larger than what is possible in a wind tunnel for sand transport, thereby alleviating the scaling issues. Nevertheless, some degree of scaling was still applied in the field experiments – approximately a 1:10 to 1:3 scale for a typical Dutch beach hut of 3 × 6 × 3 m – to make the set-up more flexible and manageable.

Scale models were placed at the beach in the morning, and the resulting deposition patterns were recorded at the end of the day, so that

Fig. 3. The set-up at one of the days (12-10-2018), testing the effect of building width and height. Note: scale model configuration, orientation and location changed between all experiments.

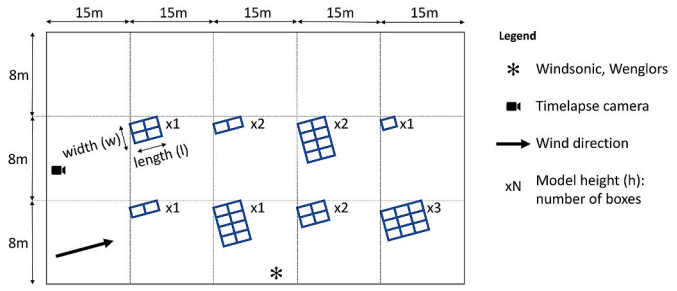

Fig. 4. A sketch (distance between scale models not to scale) of the set-up shown in Fig. 3.

Fig. 5. A map with the locations of the experiments, indicated by X on the local maps. A and B indicate locations of one-day experiments. C indicates the location of the 5-week experiment.

patterns could develop for one day. For each experiment, the orientation of the boxes was tuned to the dominant wind direction during placement of the scale models (cf. Fig. 4). For the analysis, we regard the orientation of the boxes as completely perpendicular to the wind, without taking variations in wind direction (<15° over a day, see Table 1) into account. In total there were four days during which sedimentation and erosion patterns around models were successfully recorded. Six to ten models (i.e. six to ten stacks of different dimensions) were placed on the beach every day (see Figs. 3 and 4), making for a total of 32 observations.

The experiments were mainly conducted at the Sand Motor in the Netherlands (Fig. 5). The beach is more than 500 m wide at this mega beach nourishment. Exact locations on the Sand Motor were chosen based on the prevailing wind conditions of a day to ensure large fetch lengths (more than 400 m): close to the sea for offshore wind directions (11-10-2018; 12-10-2018) and vice versa (23-10-2018). The median grain size at the Sand Motor is 335 μm (Hoonhout and De Vries, 2019). One experiment took place at the beach near Formerum, Terschelling. Here the beach is approximately 300 m wide, so in combination with the almost shore-parallel wind that occurred, aeolian sand transport was well developed. The median grain size here is approximately 200 μm (Guillén and Hoekstra, 1997). Table 1 shows an overview of the conducted experiments.

During the experiment, the wind speed and direction were measured using a 2D Windsonic ultrasonic anemometer, at 1.8 m high and with a 1 s interval. The height of the saltation layer was measured with a vertical array of 10 Wenglor laser particle counters (see Goossens et al., 2018; Hugenholtz and Barchyn, 2011). The Wenglors were placed between 5 cm and approximately 1 m above the bed, with the height of the highest sensors varying slightly to ensure the highest Wenglor was placed higher than the scale model height. The saltation layer height varied between 15 and 25 cm, so in all cases lower than the lowest scale models. Furthermore, a time-lapse with a 10 s interval was made with a camera from a height of 5 m, to be able to later identify interesting events, such as streamers or natural bedforms migrating trough the experiment area.

Additionally, a longer-term experiment was conducted, where two scale models were placed on the beach for multiple weeks: a small scale model and a full-scale model. The small scale model was a box of 0.5 × 2 × 0.5 m, so comparable in size to the one-day experiments, but more elongated in shape. The full-scale model, consisting of two shipping containers, measured 2.5 × 12 × 2.5 m, so with comparable proportions as the small scale model, but in size comparable to a real beach hut. The goals of this experiment were to determine whether the results from the small-scale one-day experiments also apply on the scale of a beach hut, and to examine morphological development over a longer period. This experiment took place in Noordwijk, The Netherlands, at a beach of approximately 150 m wide, with a measured median grain size of 300 μm (C. van IJzendoorn, pers. comm., June 8, 2020). Both scale models were placed parallel to the coast, 20 m from each other and the dune foot. The dominant wind direction was alongshore to slightly onshore, so approximately facing the short side of the scale models. Multiple storms occurred, including a heavy storm 2 days after the experiment started (Fig. 6). Results were measured at three different days (Table 2): after 1 and 3 storms days to examine the initial development, and after 5 weeks to examine the longer-term effects. Within this paper, this

Table 1
An overview of the conducted one-day experiments. For conciseness, the scale model size is indicated in boxes. Each box is 33 × 50 × 35 cm (w x l x h). The indicated wind speed is the average measured wind speed during the experiments. The wind direction variation is the difference between the dominant wind direction at the start and end of the experiment.

Date	Location	Wind speed [m/s]	Wind direction variation [°]	Variables tested	Configurations *w* x *l* x *h* [boxes]	Remarks
29-05-2018	Terschelling	6.9	*15*	*l*; *h*	3 × 1,2,4 × 1,2	bed moist due to closeness to groundwater table
11-10-2018	Sand Motor	5.9	*10*	w; h	1,2,2,4 × 1 x 1; 2,4 × 1 x 2; 1,2 × 1 x 4	bed moist due to location on intertidal beach
12-10-2018	Sand Motor	7.3	*10*	*w*; *h*	2 × 1,2,4 × 1,2; 1 × 1 × 1; 3 × 3 × 3	bed moist due to location on intertidal beach
23-10-2018	Sand Motor	9.5	*15*	*w*; *h*; *l*	1,2,4 × 1,2 × 1; 2 × 1,2 × 1,2	–

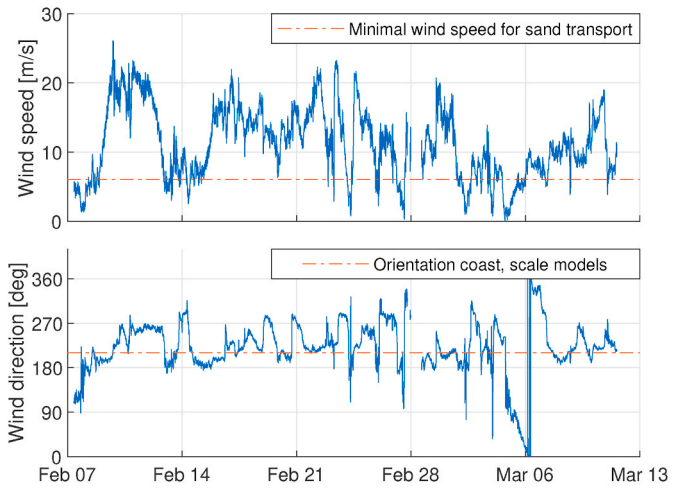

Fig. 6. Wind speed and wind direction during the 5-week experiment at Noordwijk. For comparison, wind speeds are converted to of height of 1.8 m as measured during the one-day experiments. The dashed orange line in the lower panel indicates the orientation of the coast and of the long axis of the scale models, with values above the orange line being landward blowing wind. (For interpretation of the references to colour in this figure legend, the reader is referred to the Web version of this article.)

Table 2
An overview of the measurements taken at the 5-week experiment conducted at Noordwijk. The indicated wind speeds are the average of all wind speeds higher than 6 m/s.

Date	Period	Wind Speed [m/s]	Remarks
09-02-2020	1 storm day	10	For the container, only upwind deposition was measurable
11-02-2020	3 storm days	17	Tails of full-scale model end up in dune
11-03-2020	5 weeks	13	Small scale model located in tail of full-scale model

experiment is referred to as the 5-week experiment.

Wind speed data was derived from a WindGuru measurement station at approximately 100 m from the experiment, that measures the 10-min average wind speeds at 10 m above the bed. Measurements were converted to a height of 1.8 m, as measured by the WindSonic anemometer in the one-day experiments, using a constant factor of 1.7, derived from a 3 day period for which WindSonic and WindGuru measurements at the test site were compared. To obtain a representative wind speed for days with actual sand transport, the wind speeds as displayed in Table 1 are the average of all wind speed measurements of at least 6 m/s.

The sedimentation and erosion patterns were measured using structure-from-motion photogrammetry (Fonstad et al., 2013), a technique that has been used extensively in recent years for high-resolution geomorphic surveys of beaches and dunes (e.g. Scarelli et al., 2017; Sturdivant, 2017; Van Puijenbroek, 2017). For the 1-day experiments, photos of the experimental area were taken from a height of 5 m using a camera on a telescopic stick. Photos were only taken at the end of each experiment to avoid the extra disturbance a pre-experiment survey would have created in the form of additional footsteps in the area. Given that the deposition detection method was primarily based on orthophotos rather than elevation data (see section 3.3), having a pre-experiment survey was also of lesser importance. For the 5-week experiment in Noordwijk photos were also collected with the camera on the telescopic stick, except for the last survey (11-03-2020) when photos were taken with a Phantom 4 Pro drone as, opposed to the other days, wind conditions were sufficiently mild to fly the drone. In all cases automatic white balance settings were used. Scale bars were dispersed throughout the experimental area for referencing. Additionally, for the measurement on 11-03-2020, markers were placed as ground control points and their position was measured by RTK GPS, with a vertical and horizontal accuracy of approximately 2 cm. Further details of the camera set-up, photos, and weather conditions affecting the photos can be found in Table 3.

3.2. Structure-from-motion photogrammetry

Agisoft Metashape (previously named Agisoft Photoscan) was used for the structure-from-motion (SfM) photogrammetry. Within Metashape, a 3D point cloud was calculated from overlap between photos. Based on interpolation of the point cloud, a digital elevation model (DEM) was constructed. Projecting the photos onto the DEM resulted in an orthophoto (i.e. an ortho-rectified or distortion-free top view) of the experimental area. In Metashape the accuracy was set to high for photo alignment and dense cloud generation, resulting in a horizontal resolution of approximately 2 mm for the DEM and orthophoto.

For the one-day experiments, a subset of the scale bars (between 4 and 10) was used as a reference to set the scale and improve the camera alignment in Metashape. The RMS error of these scale bars was generally below 2 mm and 3 mm for 23-10-2018. The horizontal accuracy was additionally assessed using another subset of the scale bars (at least 12), that was not used in the referencing procedure. The RMS error of this new subset of scale bars ranged between 2 and 7 mm for the different surveys, which given the 60 cm scalebar length amounts to a relative error of 1.2 per cent or less. For the 5-week experiment, we assessed the horizontal accuracy by comparing the length and width of the scale models, as measured on the orthophotos of the three measurement days. These measurements, that should all have a fixed size, differed less than 2 mm for the small scale model and less than 25 mm for the large scale model, which amounts to errors of less than 0.6 per cent.

With this accuracy and resolution, the structure-from-motion photogrammetry managed to capture the results well. The orthophoto was successful and sharp in all cases. The digital elevation models showed more variation in quality, with some completely successful, while others were locally disturbed by noise (see Fig. 7), or in case of the results of 23–10-2018, strongly disturbed by noise. This difference between DEM quality and orthophoto quality is caused by DEMs being more sensitive to projection errors than orthophotos: a difference in the vertical position of a few cm by definition changes the DEM, but it does not really affect the projection of a photo as needed for the orthophoto.

3.3. Methodology of data analysis

To determine the location and size of the deposition patterns both the orthophoto and the DEM were used, but primarily the orthophoto. Section 3.3.1 defines the types of deposition features that were measured. For these measurements, scale-model-induced deposition had to be distinguished from the unaffected beach surface. Hereto a semi-automated method was used. The edges of the deposition areas were first detected using an image recognition algorithm based on orthophoto brightness and smoothness (section 3.3.2). Next, deposition size was measured based on the detected edges and, as a quality control, these values were compared to a visual assessment of the deposition size (section 3.3.3). Finally, the measured deposition sizes were analysed to determine how they correlated with building dimensions and wind speed (section 3.3.4).

The semi-automated method for deposition detection was chosen to combine the strong points of both automated detection and detection by eye. Deposition around scale models can be recognized from a number of properties. In the first place, the deposition areas in our experiments were generally lighter than their surroundings and showed less variation in colour, because of freshly deposited sand covering shells and other surface irregularities (see also Fig. 8 and Poppema et al., 2019). Image brightness and smoothness can easily be quantified with an algorithm

Table 3
Camera and photo properties and weather conditions when taking the photos.

Date	Experiment	Camera, lens	Photo properties	Number of photos	Weather conditions
29-05-2018	1-day experiments	Canon EOS 450D with a 20 mm lens (58° horizontal angle of view)	12 Mpix jpeg	469	Sunny, dry
11-10-2018		Olympus E-PL7 with a 20 mm lens (47° horizontal angle of view)	16 Mpix raw	356	Sunny, dry
12-10-2018		Olympus E-PL7	16 Mpix raw	416	Mostly sunny, dry
23-10-2018		Olympus E-PL7	16 Mpix raw	459	Mostly cloudy, dry
09-02-2020	5-week experiment	Olympus E-PL7	16 Mpix raw	742	Cloudy, dry
11-02-2020		Olympus E-PL7	16 Mpix raw	1501	Mostly cloudy, dry but recent rain
11-03-2020		Phantom 4 Pro drone with fixed 8.8 mm lens (74° horizontal angle of view)	20 Mpix jpeg	1836	Mostly sunny, dry

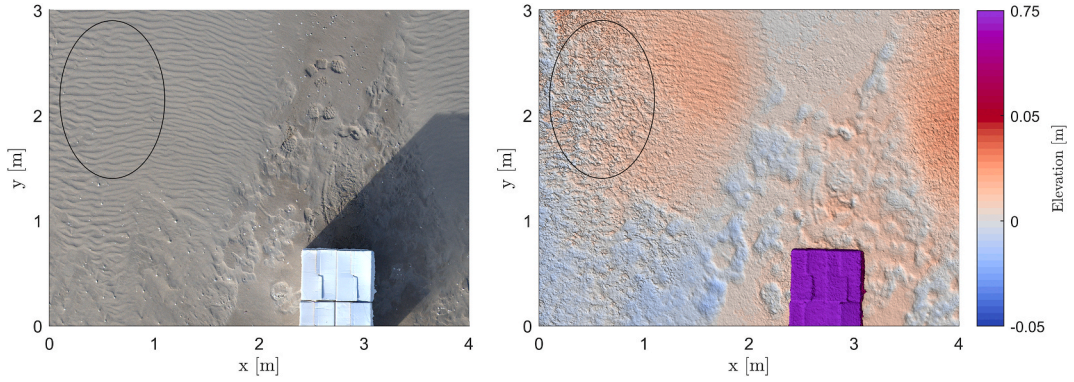

Fig. 7. Detail of the photogrammetry results, with the circle indicating an area locally disturbed by noise on the DEM (right), but still sharp on the orthophoto (left). Elevations are relative to a fitted quadratic surface of the experimental area, to highlight local differences caused by erosion and deposition (12-10-2018, scale model of 0.66 × 1x0.7 m).

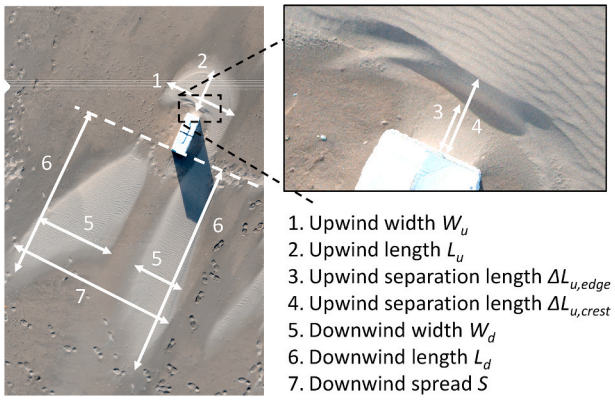

Fig. 8. The definition of the deposition size features.

from an orthophoto, and offer a consistent and repeatable criterion for identifying the edge of deposition across all set-ups and orthophotos. The human eye can more easily combine more qualitative indicators to recognize scale model-induced deposition such as its position relative to the scale models, the presence and orientation of ripples, the degree to which shells and other large particles were covered, shadows and colour differences, as well as combine it with height information from the DEM. These additional indicators were used to check the algorithmic results, to combine the consistent and repeatable results of an image recognition algorithm with the human ability to recognize patterns under changing circumstances and from multiple information sources.

3.3.1. *Deposition features of interest*

To determine the location and size of the deposition patterns, several deposition features were measured (see Fig. 8). Upwind of the scale models, a deposition area generally developed a small distance from the building, with a steep slope - close to the angle of repose - facing the scale model. Of this upwind deposition, the upwind length (L_u) was measured from the upwind building edge and the upwind width (W_u) at the widest point. The upwind separation distance (ΔL_u), so the distance between the model and deposition, was measured both at the crest of the steep slope and at the very edge of the upwind deposition (closest to the building), in both cases measured at the centreline of the scale model. Downwind, buildings generally developed two deposition tails. For each tail, the downwind length (L_d) was measured from the downwind building edge and the downwind width (W_d) at its widest location. Furthermore, the downwind spread (S), so the largest distance between the outer edges of both tails, was measured.

Height information from the digital elevation models was only used in the manual estimate of the horizontal deposition extent and not for quantifying vertical deposition size and deposition volume. Because of our focus on *initial* deposition size (so deposition dominated by the scale model effect on airflow) the precise height of deposition was of lesser importance, as vertical build-up in initial deposition areas continues with time, where transport rate and duration will influence how fast this vertical buildup occurs. Indeed, deposition heights varied between experiments, ranging from only being visible as a colour difference without measurable vertical elevation change, to occasionally more than 10 cm. As argued in section 2.3, the effect of wind speed (as proxy for transport rate) on *horizontal* size of initial deposition areas is expected to be approximately linear, and such effects of wind speed are examined in

the Results section.

3.3.2. Edge detection algorithm

To distinguish the deposition patterns in the one-day experiments, an edge detection algorithm was used. This algorithm is based on the orthophotos, because deposition varied greatly in height, and occasionally consisted of a very thin layer that was only visible on the orthophotos and not on elevation maps. Thresholding is applied to the orthophotos to distinguish the lighter and smoother deposition areas from the undisturbed bed. The workflow to detect these areas consists of three steps: image preparation, binarization and edge detection (Fig. 9). For the 5-week experiment, with larger deposition heights and lower contrast due to drier background surfaces, this algorithm was not used, and measurements were primarily based on the elevation map.

As image preparation, the orthophoto of the area was downscaled to a 1 cm resolution and then converted to greyscale. Next, the image intensity was normalized. The area (pixels) with boxes was filtered out, to only look at the sandy areas. The remaining image intensity was normalized, by assigning pixels that were 3 standard deviations darker/brighter than the mean as black resp. white (value 0 resp. 255).

This grayscale image was binarized, to divide the area in 'deposition areas' and 'rest'. Deposition areas were generally lighter than their surroundings, so pixels were classified as deposition if they were lighter than some threshold T. To take the lower variation of deposition areas into account, the value of T was increased in areas with large variation. This was implemented using an adapted version of the Sauvola algorithm (Sauvola and Pietikäinen, 2000; Shafait et al., 2008). Further details can be found in the appendix.

Finally, edge detection was used to focus on the largest detected areas. Hereto all areas with a surface area of less than 0.25 m^2 (2500 pixels) were removed. Next, the remaining areas were merged if they were less than 4 pixels (4 cm) apart and the outer edges of these areas were plotted.

3.3.3. Deposition measurement and correction

From the detected deposition edges (Fig. 9), the areas of interest were selected, so the upwind deposition and the downwind deposition areas. Then these areas were measured: the width, length and separation distance of the upwind deposition, and the width, length and spread of the downwind deposition areas, as described in section 3.3.1. This is sketched in Fig. 10A.

Next, as a control, the extent of the deposition was also manually estimated based on visual identification of the deposition area (Fig. 10B and C). This visual identification was based on the degree to which shells and other large particles were covered by sand, shadows and colour differences in the orthophoto, the location with respect to the scale models, the presence and orientation of ripples, and height information from the DEM. Fig. 11 shows a more detailed example, to illustrate how shells, ripples and colour differences were used to estimate deposition dimensions.

The measurements of the automatically detected deposition areas were compared to the manually derived estimate (Fig. 10D and E). If the results of the manual estimate was significantly different (more than 10%), automatically detected edges were further examined. Automatic dimensions were kept in case they were plausible: deposition could be quite diffuse, so sometimes the edge of the detection could be quite different, but still realistic. The manual measurement was used in case the automatic edge detection was clearly incorrect.

For the upwind separation distance at the crest, the edge detection algorithm was never used. This was always measured by hand based on the DEM, as the algorithm did not include height information. For the upwind separation distance at the edge (see Fig. 8) manual correction was needed in nearly all the cases: due to the smaller feature size and reflections and shadows from the scale models, the edge detection algorithm did not perform well here. For the other features, this correction was needed in 25 per cent of the cases.

3.3.4. Relating deposition size to building dimensions and wind speed

After determining the deposition size, the effect of separate building dimensions (w, h and l) and compound scaling lengths (R and B, see eqs. (1) and (2)) on the horizontal deposition size was examined. For the downwind length and width, the deposition size was based on the average value of both tails. In case only one tail has been measured, that value was used. The strength of these effects was determined using linear regression, based only on the one-day experiments with boxes. Results of the 5-week experiment were compared to the one-day experiment results, but both small-scale and full-scale results were excluded from the regression to serve as first validation for how well the derived relationships perform for longer periods and full-scale buildings.

The effect of wind speed was examined next. From the theory, measured downwind deposition length is expected to increases linearly with wind speed – if the measurement duration and other conditions are similar and the bed remains flat enough that initial conditions still apply. For the other measures of deposition size, the effect of wind speed is not known yet. To determine which deposition dimensions were affected by the wind speed, the effect of building dimensions on deposition was first removed by dividing the deposition dimensions by B. Then the residual variation was examined: we assessed for which deposition dimensions a significant linear correlation ($\alpha = 0.01$) existed between wind speed and the deposition dimension divided by B. For the deposition dimensions with significant wind speed effects, a new trend for B was calculated, compensated for the effect of wind speed. Hereto correlation was examined between B and the deposition dimensions divided by the relative wind speed $U/\bar{U}$ (so the wind speed divided by the average wind speed of the four days).

4. Results

The deposition patterns of the one-day experiments (Fig. 12A–D) and of the 5-week experiment at Noordwijk (Fig. 12E and F) were measured to determine how deposition size depends on the building dimensions. The deposition patterns around the scale models were substantial in size: the total deposition length (from upwind to downwind edge) and width could be an order of magnitude larger than the horizontal scale model dimensions (see e.g. Fig. 12D). Next, the effect of the building dimensions on the horizontal deposition dimensions was examined in more detail. Table 4 shows how the dimensions of the one-day scale models correlate with the deposition dimensions. The scale model width

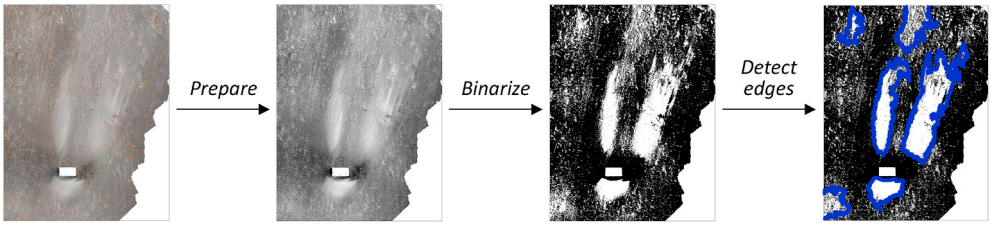

Fig. 9. The edge detection algorithm. NB: The original orthophoto (left image) is in colour, there is just very little colour visible. After preparation it converted to grayscale. (For interpretation of the references to colour in this figure legend, the reader is referred to the Web version of this article.)

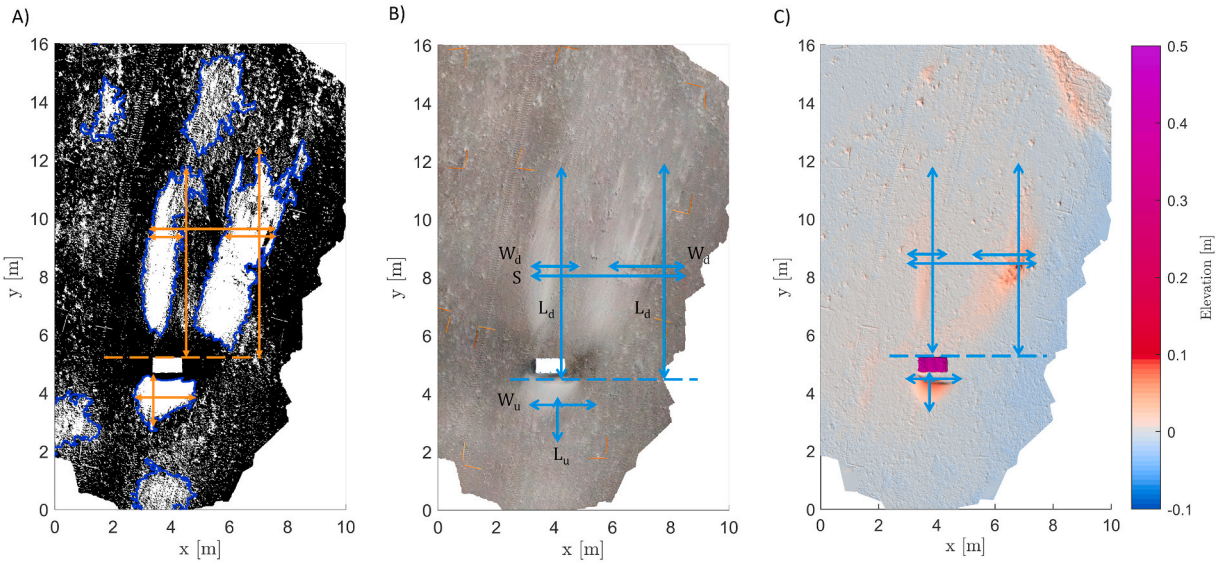

D)

Compare measurements

Less than 10% difference between algorithmic and manual measurement? — *Yes* → Keep algorithmic measurement

No ↓

Algorithmic measurement plausible? — *Yes* → Keep algorithmic measurement

No ↓

Use manual measurement

E)

Dimension		Measurement [m]		Value used
		Algorithm	Manual	
W_u		2.1	2	Algorithm: values similar
L_u		1.8	1.4	Manual measurement of orthophoto
Δl_u	edge		0.17	Manual measurement of orthophoto
	crest		0.4	Manual measurement of DEM & orthophoto
W_d	left	1.2	1.4	Algorithm: value plausible
	right	1.8	2.2	Algorithm: value plausible
L_d	left	6.5	6.5	Algorithm: values similar
	right	7.2	6.6	Algorithm: values similar
S		4.35	4.45	Algorithm: values similar

Fig. 10. The measurement of deposition size, indicated by arrows on the orthophotos and DEM for one scale model (29-05-2018, model of 1 × 0.5 × 0.35 m). A) Measurement of the algorithmically detected edges, here plotted in blue on the binarized orthophoto. B) Manual measurements on the orthophoto, based on visual inspection. C) Manual measurements on an elevation map. Elevations are relative to a fitted quadratic surface, to highlight local differences caused by erosion and deposition. D) The workflow for comparing algorithmic and manual measurements. E) Example of the determination of deposition size from algorithmic and manual measurements. (For interpretation of the references to colour in this figure legend, the reader is referred to the Web version of this article.)

had far more effect on the deposition dimensions than the model height and length. Although model height has little predictive value on its own, using both width and height information - by means of *R* or *B* - substantially improves the correlation. Of the two, *B* (eq. (2)) scores better than *R* (eq. (1)). This effect of *B*, based on only the one-day experiments, is also plotted as a trendline in Fig. 13.

Fig. 13 also shows the measurements of the 5-week experiment, including both a full-scale model (Fig. 12E) and a small scale model (Fig. 12F). Three measurements were taken during the 5-week experiment: after 1 storm day, 3 storms days and 5 weeks. For the full-scale model, deposition developed more slowly: after 1 storm day, it exhibited no measurable downwind deposition, so only the upwind deposition dimensions were measured and plotted in Fig. 13. Notable for the result after 3 days is that the wind direction was at an angle of about 45° with respect to the scale models (Fig. 6), affecting the deposition development (see Fig. 14A). Deposition dimensions have been measured in the direction of the container in this case, so at an angle to the wind. The deposition tails extended up to the dune toe, making tail lengths difficult to measure. Therefore the measured lengths up to the dune foot are indicated as a lower limit. Notable for the result after 5 weeks is that the small scale model is situated exactly in the deposition tail of the container due to the wind direction, causing it to become partially

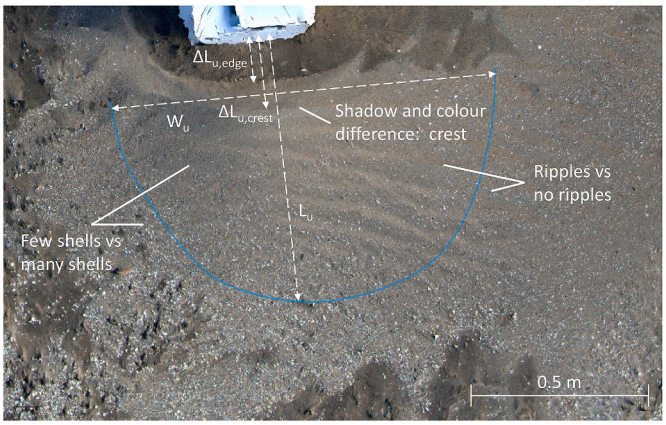

Fig. 11. Detail of an orthophoto of upwind deposition, showing how shells, ripples and colour differences were used to distinguish and measure the deposition size (23-10-2018, model of 0.33 × 0.5 × 0.35 m). The blue line indicates the best manual estimate of the deposition edge. (For interpretation of the references to colour in this figure legend, the reader is referred to the Web version of this article.)

buried (Figs. 12F and 14).

Comparing the 5-week experiment to the 1-day experiment, measurements from the first days of the 5-week experiment exhibit the best agreement with the 1-day experiments. Of the measurements taken after one storm day, 5 fall within the confidence interval of the 1-day experiment, while two are just outside the interval. After three storm days, mostly with wind at an angle to the scale models, 5 measurements are within the confidence interval, and 5 above the interval. After 5 weeks, 2 measurements are within the interval, 2 below the interval and 5 above it. Especially measured lengths are larger than expected: the downwind length after 3 storm days and the upwind and downwind length after 5 weeks are all well outside the confidence interval. This is likely due to the combination of strong wind (see Table 2 and Fig. 6) and a longer period compared to the one-day experiments.

Therefore, the effect of wind speed was examined next. Within the one-day experiments, the deposition size, scaled (divided) by *B*, generally increased with wind speed (not shown). For the downwind length and downwind spread, this effect was significant at $\alpha = 0.01$. Therefore, we made new plots for the effect of *B* on deposition size, in which we aimed to compensate for these wind speed effects. Dividing the deposition sizes by the relative wind speed (so $U/\bar{U}$ of the four days) improves the correlation of only the upwind length, downwind length and downwind spread (Fig. 15 and the last column of Table 4). In addition,

Table 4
Determination coefficients (R^2 values) for the best linear fit between building dimensions and deposition dimensions of the one-day experiments. For B* the deposition dimensions have been divided by the relative daily wind speed $U/\bar{U}$. Individual R^2 values that are not significant at an $\alpha = 0.01$ level are indicated between brackets.

	w	h	l	R	B	B*
Upwind width (W_u)	0.51	(0.03)	(0.02)	0.44	0.60	0.54
Upwind length (L_u)	0.38	(0.05)	(0.08)	0.38	0.48	0.54
Upwind separation distance edge ($\Delta L_{u,edge}$)	(0.12)	0.29	(0.03)	0.51	0.38	0.17
Upwind separation distance crest ($\Delta L_{u,crest}$)	0.62	0.28	(0.01)	0.77	0.85	0.64
Avg downwind width (W_d)	0.59	(0.05)	(0.07)	0.51	0.68	0.66
Avg downwind length (L_d)	(0.20)	(0.05)	(0.09)	0.29	0.30	0.47
Downwind spread (S)	0.32	0.44	(0.06)	0.64	0.60	0.73
Average R^2 value	0.39	0.17	0.05	0.51	0.56	0.54

Fig. 12. Examples of deposition around scale models, with arrows indicating the (dominant) wind direction. A) Small scale models of different length, with upwind deposition and deposition tails visible as lighter areas (29-05-2018). B) The nearest small scale model of photo A from another angle. C) Deposition with a considerable elevation difference (23-10-2018). D) An orthophoto of deposition (12-10-2018). E) The full-scale model of the 5-week experiment, showing deposition, erosion and undercutting under the upwind side of the container (11-03-2020). F) The small scale model of the 5-week experiment, half-buried and with a deposition tail downwind of the model (11-02-2020).

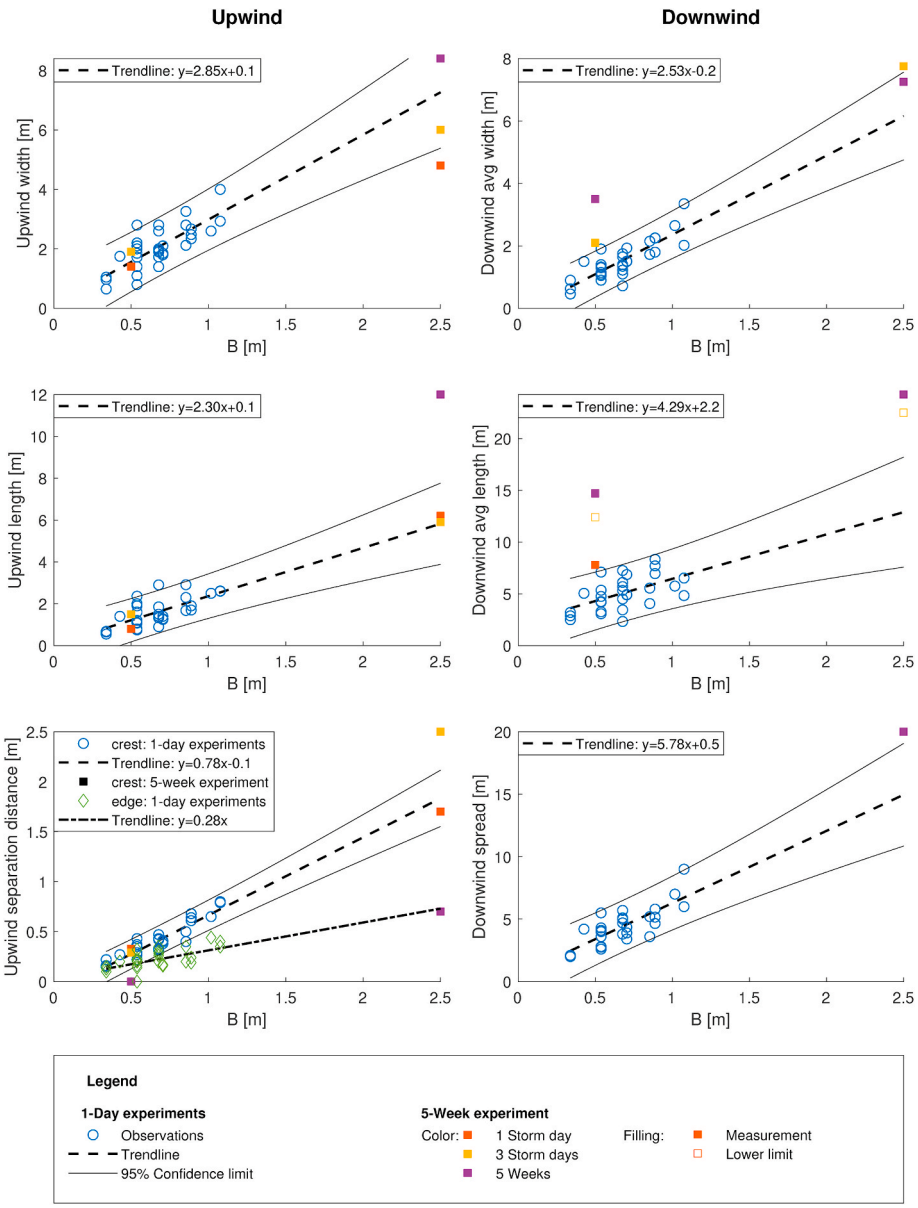

Fig. 13. Experimental results showing the effect of the building scaling length B on deposition size. Plotted trendlines are only based on the one-day experiments, squares indicate results of the 5-week experiment with the small scale model (at B = 0.5 m) and full-scale model (at B = 2.5 m) in Noordwijk.

this scaling improves the match between the container results and the empirical trendlines.

To test to what extent the power of 1/3 and 2/3 in B (eq. (2)) actually match the data, we also fitted eq. (6) to the data, with x denoting any of the deposition dimensions, and power γ and 1-γ to have powers with a summed value of 1 (Wilson, 1979). Averaged over all the deposition dimensions, the maximum determination coefficient (R^2) was obtained with a value of $\gamma = 0.63$, so very close to the 2/3 used in B. The R^2 value increases with less than 0.01 and the adjusted R^2 value – where the value of R^2 is adjusted for the number of terms in a model to prevent over-fitting (Theil, 1961) – actually decreases, further supporting the original powers in B.

$$x = \alpha + \beta \cdot w^{\gamma} \cdot h^{1-\gamma} \tag{6}$$

5. Discussion

5.1. Experimental set-up: scaling and uncertainties

In this experiment, scale models were placed at the beach in order to examine aeolian deposition around buildings. Using scale models, only the building size was scaled and all other conditions (wind speed, grain size, saltation height, etc.) were not. The downside of this approach is that it can introduce scaling issues. Due to the high density of sand compared to air, grains do not instantaneously follow airflow but take some time and distance to adapt. Relative to the size of buildings and airflow patterns, this adaptation length becomes larger. Furthermore, sand transport occurs mostly in the saltation layer near the bed and decreases with elevation, so sand transport over small scale models may be larger than sand transport over actual buildings. This implies that deposition behind a small scale model might over-estimate deposition behind a full-scale building. However, measurements with a vertical array of Wenglor sensors showed that our smallest scale models were already higher than the saltation layer, hence this is assumed to have

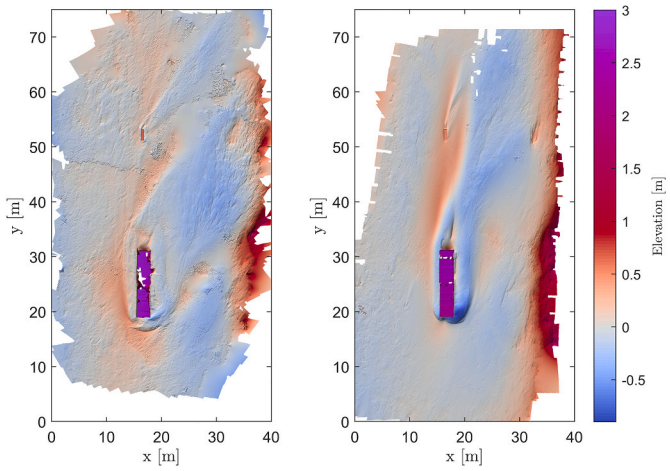

Fig. 14. Elevation maps of the deposition around the 5-week scale models at Noordwijk. The small scale model is located around x = 15, y = 50. The elevation is relative to a fitted quadratic surface to highlight local disturbances. Higher elevations at the right hand edge are the toe of the dune. Left: elevation map after 3 storm days. Right: elevation map after 5 weeks.

very little effect in our experiments.

In experiments similar to ours, on the deposition of snow around scaled buildings in a natural environment, scaling issues only played a small role (Liu et al., 2018; Oikawa and Tomabechi, 2000; Thiis, 2003; Thiis and Gjessing, 1999). In addition, strong scaling issues within our experiments would likely be visible as discontinuities in the relations found, or relations breaking down at smaller scales. Our relations fit the entire range of the one-day experiments and also match the results obtained around the full-scale model after the first days of the 5-week experiment quite well. Furthermore, if results from the 5-week experiment deviated from the relations, same-day measurements around the full-scale model and the small scale model usually deviated in a similar manner (see in Fig. 13 the upwind separation distance after 5 weeks, and the downwind deposition length and width). Together, this suggests that the importance of scaling issues for our experiment is limited, with likely sand transport following the same paths, predominantly around (not over) buildings, similar airflow around scale models and buildings and these airflow patterns similarly controlling the deposition size and location.

The morphological development was further affected by variations in transport conditions. As expected, deposition patterns developed more quickly on days with larger wind speeds, resulting in somewhat larger horizontal deposition dimensions. This is especially visible for the downwind deposition length and spread in the one-day experiments (Table 4), fitting the hypothesis that the initial downwind length scales linearly with wind speed. For the downwind spread, the increasing deposition length is likely the underlying cause: for diverging tails, downwind spread increases automatically with length. For the other horizontal deposition sizes, there was no significant effect from wind speed.

For the 5-week experiment, the wind speed effect largely explains the deviations of the measured deposition dimension from the empirical relations, especially for the downwind deposition length and spread (see also Fig. 15). Moreover, the measurements were taken after multiple days to a month, thereby giving the morphology a long time to develop, further explaining the larger deposition. The exceptional weather conditions during the 5 weeks - multiple storms in a month with an almost constant wind direction, dominantly alongshore directed and hardly any rain - resulted in abundant aeolian transport that created deposition patterns that are most likely exceptionally well developed in terms of deposition size. Normally, frequent changes in wind direction lead to a

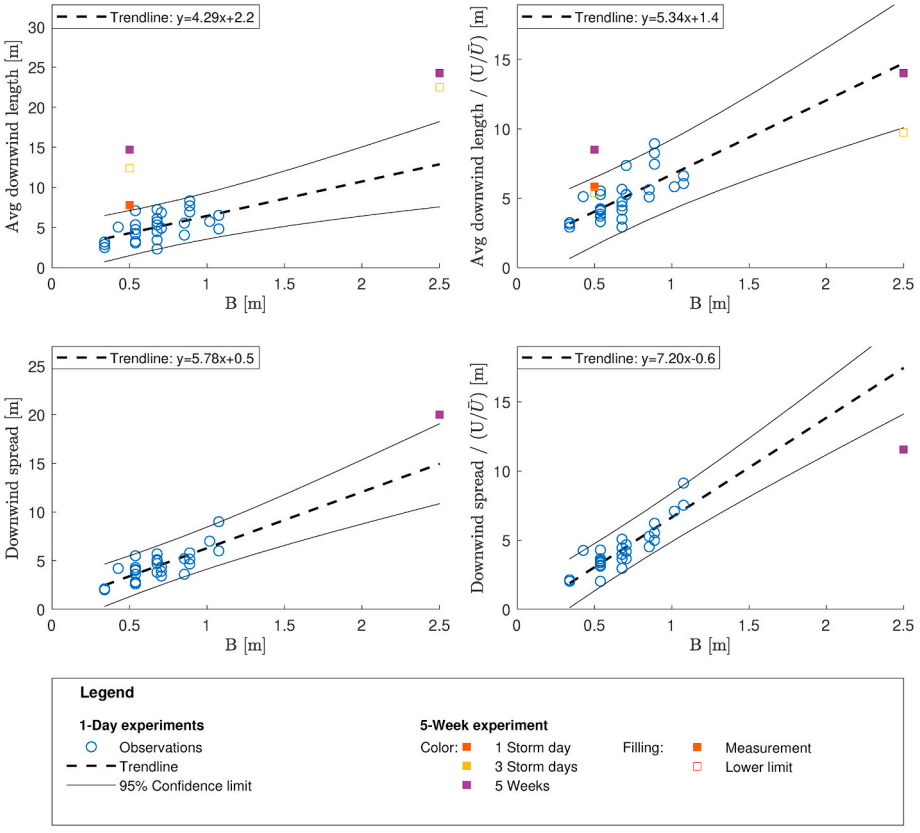

Fig. 15. The effect of building scaling length B on deposition size, compensated for wind speed. Trendlines are only based on the one-day experiments, squares indicate results of the 5-week experiment with the small scale model and full-scale model in Noordwijk. NB: subplots on the left are equal to Fig. 13.

reshaping of morphological patterns, thereby limiting the maximum deposition development.

The separation distance of the upwind deposition observed in the full-scale test after 3 days of storm conditions was also larger than predicted by the empirical relation. This could be related to the oblique wind angle and very elongated scale model shape: this increased the effective wind-facing surface, possibly creating a larger recirculation vortex (see Fig. 2) and thereby increasing the separation distance. This also indicates that wind at oblique angles to a building causes different deposition patterns than perpendicular winds (see also the results in Fig. 14), so this should be examined further. Conversely, the upwind separation distance of the crest after a month was considerably smaller than predicted. This may be explained by the strong topographic change that occurred on the upwind side of the full-scale model. Erosion undercutted the front of the model, causing the model to tilt down, while simultaneously strong deposition occurred upwind of the model. Together, this decreased the model height relative to the surrounding bed level. This would decrease the size of the recirculation vortex upwind of the model, over time allowing the upwind deposition to extend further toward the full-scale model.

The 5-week experiment further demonstrated that the physical size of scale models influences the time it takes for erosion and deposition to develop. The small scale model showed clear deposition after one storm day, while the full-scale model showed only starting upwind deposition (lower than in front of the small scale model, and no crest visible), and no visible downwind deposition yet. This implies that the results of the small-scale one-day experiments may be interpreted as more or less representative of the state around full-scale buildings after a somewhat longer period.

The comparison of deposition patterns of the 5-week experiment to those predicted by the empirical relations for *initial* deposition size also revealed the extent to which these relations are meaningful for longer-term morphological development. Here *initial* refers to the situation in which the building is situated on a generally flat bed, so that the building itself dominates the airflow patterns and sediment dynamics. The 5-week experiment examined deposition development around a small and a full-scale model and for a longer period, which resulted in substantial deposition also in the vertical dimension (up to 0.5 m). The horizontal size of deposition patterns after 1 and 3 days of the 5-week experiment, matched the empirical relations reasonably well, although better for the small scale model than for the full-scale model (Fig. 13). The deposition areas observed after 5 weeks were generally larger than predicted by the relations. The larger deposition area could be partially attributed to the high wind speeds (Table 2), but given the considerable bed level change at this point (Fig. 14), the situation after 5 weeks could likely no longer be characterized as initial deposition.

Although initial deposition areas grow with wind speed and with time, this growth will not continue indefinitely. Over time, as the deposition height increases, the topography itself starts to affect airflow, partially cancelling out airflow effects induced by the building (McKenna Neuman and Bédard, 2015; McKenna Neuman et al., 2013). From the reasonable match between the results of the 5-week experiment and the windspeed-corrected empirical relations for initial deposition size, it seems that horizontal deposition growth after the formation of initial deposition is relatively limited. Hence, the empirical relationships of this study, with the exception of the upwind separation distance, can reasonably be applied to approximate longer-term deposition size.

Finally, in the correction for wind speed effects, wind speed is used as a proxy for sediment transport rate, as patterns develop more quickly with larger transport rates. However, also other factors determine the transport rate, such as fetch length, soil moisture and grain size (e.g. Bauer et al., 2009; Delgado-Fernandez, 2010; Kok et al., 2012). With experiments on different days and different locations this is considered a source of the scatter around the derived relations. Similarly, variation in wind speed or direction during a day and differences in the transport duration between days may have caused some further scatter.

Apart from variation in these environmental conditions, the measurement accuracy also has some contribution to the scatter. As illustrated by Fig. 10, there is uncertainty in identifying the edges of deposition patterns, and sometimes there could be quite a wide range of plausible locations for the border between deposition and undisturbed beach (decimetres up to occasionally metres). To limit the subjectivity in edge detection, an algorithm was applied to detect the edge, and visual identification was only applied in case of clearly erroneous edge detection.

5.2. *Effect building dimensions on deposition size*

In the observed patterns of erosion and deposition around the small-scale and full-scale models, deposition dominated and occurred in a large area around the models, while erosion seemed to be restricted to the area directly around the models in most cases (with erosion areas judged from darker areas, areas with more shells or elevation data for the one-day scale experiments (Poppema et al., 2019) and from elevation data for the 5-week experiments). There are several reasons for this. The strong acceleration of wind forced by a building only takes place directly around a building, leading to a local increase of sediment transport rates and erosion. The downwind deceleration and decrease of sediment transport rates toward undisturbed equilibrium conditions is a more gradual process, thereby taking place over a longer distance. However, the amount of deposition and erosion also varied between the cases. For instance, on day 2 and 3 of the small-scale experiments, erosion was further limited by soil moisture. Conversely, the small-scale experiments of day 4 (23-10-2018), conducted during high wind speeds, and the 5-week experiment, experienced strong erosion at the upwind building edges, resulting in undercutting of the scale models (Fig. 12E). Overall, the observed dominance of deposition over erosion shows that the buildings do not only redistribute sand locally (i.e. from erosive to accreting areas), but that they can also capture sand that would otherwise be transported further downwind.

In the experiment, the upwind separation distance of the crest showed exceptionally good correlation with B, while the upwind separation distance of the edge showed more variation. This fits the results of Tsoar (1983), who found that in a wind tunnel the crest position of echo dunes in front of a cliff was relatively fixed, while the edge position grew toward a cliff with dune height. Together, these results imply that the location of the crest of the upwind deposition is determined by the building and by the airflow structures, while the edge depends also on the deposition height and angle of repose and hence on a range of other factors (most notably the experimental duration and sediment transport rate). This is further supported by the fact that the relationship we found for the morphological upwind separation distance of the crest ($0.1 + 0.8B$) is similar to the relations from earlier experiments on the aerodynamic upwind separation distance: $R_u = 0.7\sqrt{wh}$ and $R_u = 0.8w^{0.4}h^{0.6}$ (Beranek, 1984; Martinuzzi and Tropea, 1993).

The length of deposition features showed the lowest correlations with building dimensions, both for the upwind and downwind deposition - although still clearly statistically significant at $\alpha = 0.01$. A part of this can be contributed to the wind speed: as demonstrated in the theory-section, wind speed affects deposition length more strongly than deposition width. With deposition length depending more strongly on local conditions, the correlation with building properties becomes lower.

Overall, the new scaling length B for the deposition around buildings (eq. (2)) correlates well with the measured deposition dimensions. In earlier literature (Schulman et al., 2000; Wilson, 1979), length scale R (eq. (1)) was used as a scaling factor for aerodynamic flow structures around buildings. For B, the contribution of building width is set larger, because building width is more important than building height for the disruption of sediment transport: sediment transport occurs mostly close to the bed. This physical reasoning, in combination with the fact that B is

a simpler equation than R, yet correlates stronger with the one-day experiments, and the very close fit for B with the powers as calibration parameters (eq. (6)) as well as the good match with 5-week and larger-scale container results, instils confidence that B is an improvement over R for describing the dependence of deposition patterns on building dimensions.

The small scale models, on which the empirical relations between deposition size and building scaling length B are based, had aspect ratios (w/h) between 0.2 and 3.4. Because the *type* of airflow pattern developing around a building (see Fig. 2) also depends on the aspect ratio, these relations should not be used for any arbitrary building aspect ratio. When the aspect ratio of a building increases, relatively more wind will be diverted over the building instead of along its sides, causing a lowering of the stagnation point at the upwind building face (see Fig. 2). Eventually, for very wide buildings ($w/h > 10$), flow patterns change completely, with also longitudinal vortices developing over the building (Martinuzzi and Tropea, 1993). As a result, the scaling of the upwind and downwind separation length with building width as reported by Martinuzzi and Tropea (1993) changes around $w/h = 4$, and especially the upwind separation length subsequently becomes almost width-independent for $w/h > 6$. Given these results and the range of aspect ratios tested in our scale experiments, we suggest limiting the application of our empirical relations for predicting deposition dimensions to buildings with aspect ratios between 0.2 and 4.

The new quantitative knowledge on the horizontal size of deposition around a building can be used to indicate the local area of influence of a beach building. As a next step, the long-term implications of these effects for the larger beach-dune area should be determined, by examining the interaction between local deposition and beach-dune dynamics. Furthermore, building-induced deposition on walkways, terraces and beach entrances often forms a hindrance to the public or building owners (Jackson and Nordstrom, 2011). The empirical relations on deposition size can be used as a guideline to place buildings or beach infrastructure in such a way that the hindrance from deposition and the need for sediment removal is minimized, for instance as a minimum required distance between a building and a beach entrance.

6. Conclusions

Block-shaped scale models of buildings were placed at the beach to study how the size of initial aeolian deposition patterns around buildings depends on building dimensions. These deposition patterns are of considerable size: their length and width are up to an order of magnitude larger than the horizontal building dimensions. The deposition patterns are caused by the airflow patterns around buildings, which form a horseshoe vortex. While the size of building-induced airflow patterns scales with both building width (w, measured perpendicular to the wind direction) and building height (h), related sedimentation patterns scale more strongly with the width of the building. This is explained by sand transport mostly occurring close to the bed, so little sand is blown over buildings irrespective of building height. This difference is reflected by the new scaling length B for deposition around buildings, with $B = w^{2/3} \cdot h^{1/3}$ to combine the effects of building width and building height.

In scale experiments with scale models of buildings placed at the beach for a single day, B scaled linearly with the horizontal dimensions of upwind and downwind deposition patterns, while building length had very little effect. Fitted relations between B and the horizontal deposition dimensions were statistically significant and showed good correlation. The good match between these relations and the deposition development around a full-scale model that was tested for 5 weeks, supports the use of B and these relations for predicting the horizontal deposition size around buildings at the beach. The w/h ratios of the tested scale models and the behaviour of airflow around buildings suggest these relations are applicable for buildings with a w/h ratio between approximately 0.2 and 4.

Author statement

Daan Poppema: Methodology, Investigation, Formal analysis, Writing – original draft, Writing – review and editing. **Kathelijne Wijnberg:** Conceptualization, Supervision, Writing – review and editing, Project administration, Funding acquisition. **Jan Mulder:** Investigation, Writing – review and editing, Supervision, Funding acquisition. **Sander Vos**: Investigation, Recourses. **Suzanne Hulscher:** Writing – review and editing, Supervision.

Declaration of competing interest

The authors declare that they have no known competing financial interests or personal relationships that could have appeared to influence the work reported in this paper.

Acknowledgements

This research forms part of the ShoreScape project. The 5-week experiment at Noordwijk forms part of the larger Scanex experiment, organized by the CoastScan project. ShoreScape is funded by the Netherlands Organization for Scientific Research (NWO), contract number ALWTW.2016.036, co-funded by Hoogheemraadschap Hollands Noorderkwartier and Rijkswaterstaat, and in kind supported by Deltares, Witteveen&Bos, and H+N+S. CoastScan is also funded by NWO under project number 2018/STW/00505023 and focuses on coastal variability and resilience and the influence of natural and antropogenic factors on these properties. We also want to thank Rijkswaterstaat for the logistic support during the experiment at the Sand Motor, the municipality of Noordwijk for their support on the Scanex experiment, Vaclav Hornik of Windguru.cz for sharing wind data from Noordwijk and Christa van IJzendoorn for sharing grain size data from Noordwijk. Furthermore, we thank Jan Willem van Dokkum and Mieke Kuschnerus for their excellent help during the preparation and execution of the experiments. In addition, we are grateful to Janneke van Bergen, Paran Pourteimouri, Geert Campmans, Sara Dionísio António, Weiqiu Chen, Joost Kranenborg, Mariëlle Rotteveel, Sam de Roover, Ton van der Heide and the Oerol festival organization for their assistance with the experiments.

Appendix

The Sauvola algorithm (eq. (7)) is a local thresholding technique, with the local threshold T depending on the mean m and standard deviation σ of the intensity in a window centred around the pixel. R is the dynamic range of the standard deviation, so the highest value of σ for the entire image; k is a calibration parameter. This algorithm was originally developed for text recognition (Sauvola and Pietikäinen, 2000), but has also been used in a range of medical and engineering applications (e.g. Kim et al., 2017; Senthilkumaran and Vaithegi, 2016).

In its original application, the features of interest (letters) are darker than the background and exhibit more variation. In our case the opposite applied: deposition areas were lighter and exhibited less variation. Therefore, equation (8) was used instead. Conceptually this resulted in the same behaviour: the threshold is equal to m in the most promising area and stricter by a factor k in the least promising area. For parameter k, a value of 0.8 was used. The mean and standard deviation were calculated in a neighbourhood around the pixel of interest. Here, two different window sizes were

actually used. For the mean a window of 4 × 4 m was used, to ensure that the window was larger than deposition features (otherwise deposition could not be distinguished by being lighter than the mean). For the standard deviation, a window of 30 × 30 cm was used, so this is really the variation of the area directly around the pixel itself.

$$T = m\left(1 + k\left[\frac{\sigma}{R} - 1\right]\right) \tag{7}$$

$$T = m\left(1 + k\frac{\sigma}{R}\right) \tag{8}$$

References

ASHRAE, 2005. 2005 ASHRAE handbook: Fundamentals - SI edition. American Society of Heating Refrigerating and Air-Conditioning, Atlanta.

Bagnold, R.A., 1941. The Physics of Blown Sand and Desert Dunes. Chapman & Hall, Londen.

Bauer, B.O., et al., 2009. Aeolian sediment transport on a beach: surface moisture, wind fetch, and mean transport. Geomorphology 105 (1), 106–116.

Beranek, W., 1984. Wind environment around single buildings of rectangular shape. Heron 29 (1), 4–31.

Delgado-Fernandez, I., 2010. A review of the application of the fetch effect to modelling sand supply to coastal foredunes. Aeolian Res. 2 (2–3), 61–70.

Dong, Z., Liu, X., Wang, H., Zhao, A., Wang, X., 2003. The flux profile of a blowing sand cloud: a wind tunnel investigation. Geomorphology 49 (3), 219–230.

Duthinh, D., Simiu, E., 2011. The Use of Wind Tunnel Measurements in Building Design. In: Lerner, J.C. (Ed.), Wind Tunnels and Experimental Fluid Dynamics Research. InTech, pp. 282–300. https://doi.org/10.5772/18670.

Fackrell, J., 1984. Parameters characterising dispersion in the near wake of buildings. J. Wind Eng. Ind. Aerod. 16 (1), 97–118.

Fonstad, M.A., Dietrich, J.T., Courville, B.C., Jensen, J.L., Carbonneau, P.E., 2013. Topographic structure from motion: a new development in photogrammetric measurement. Earth Surf. Process. Landforms 38 (4), 421–430.

García Romero, L., et al., 2016. Urban-touristic impacts on the aeolian sedimentary systems of the Canary Islands: conflict between development and conservation. Island Stud. J. 11 (1), 91–112.

Goossens, D., et al., 2018. Field testing, comparison, and discussion of five aeolian sand transport measuring devices operating on different measuring principles. Aeolian Res. 32, 1–13.

Guillén, J., Hoekstra, P., 1997. Sediment distribution in the nearshore zone: grain size evolution in response to shoreface nourishment (island of terschelling, The Netherlands). Estuar. Coast Shelf Sci. 45 (5), 639–652.

Hansen, A.C., Cermak, J.E., 1975. Vortex-containing Wakes of Surface Obstacles, Project THEMIS Technical Report. Colorado State University, Fluid dynamics and diffusion lab, Fort Collins, USA.

Hoonhout, B., De Vries, S., 2019. Simulating spatiotemporal aeolian sediment supply at a mega nourishment. Coast Eng. 145, 21–35.

Hoonhout, B.M., Van Thiel de Vries, J., 2013. Invloed van strandbebouwing op zandverstuiving, Adviezen voor vergunningverlening (In Dutch). Deltares, Delft.

Hoonhout, B.M., Waagmeester, N., 2014. Invloed van strandbebouwing op zandverstuiving, een verkenning naar methoden, meetgegevens en modellen (in Dutch). Deltares, Delft.

Hugenholtz, C.H., Barchyn, T.E., 2011. Laboratory and field performance of a laser particle counter for measuring aeolian sand transport. J. Geophys. Res.: Earth Surf. 116 (F1).

Hunt, J., 1971. The effect of single buildings and structures. Phil. Trans. Roy. Soc. Lond. A 269 (1199), 457–467.

Iversen, J.D., et al., 1990. The effect of a roughness element on local saltation transport. J. Wind Eng. Ind. Aerod. 36, 845–854.

Iversen, J.D., Wang, W.P., Rasmussen, K.R., Mikkelsen, H.E., Leach, R.N., 1991. Roughness Element Effect on Local and Universal Saltation Transport. Vienna, pp. 65–75.

Jackson, N.L., Nordstrom, K.F., 2011. Aeolian sediment transport and landforms in managed coastal systems: a review. Aeolian Res. 3 (2), 181–196.

Kim, H., Ahn, E., Cho, S., Shin, M., Sim, S.-H., 2017. Comparative analysis of image binarization methods for crack identification in concrete structures. Cement Concr. Res. 99, 53–61.

Kok, J.F., Parteli, E.J.R., Michaels, T.I., Karam, D.B., 2012. The physics of wind-blown sand and dust. Rep. Prog. Phys. 75 (10), 106901. https://doi.org/10.1088/0034-4885/75/10/106901.

Kothari, K.M., Peterka, J.A., Meroney, R.N., 1979. Stably Stratified Building Wakes. Colorado State University, Fluid dynamics and diffusion lab, Fort Collins, USA.

Kothari, K.M., Peterka, J.A., Meroney, R.N., 1986. Perturbation analysis and measurements of building wakes in a stably stratified turbulent boundary layer. J. Wind Eng. Ind. Aerod. 25 (1), 49–74.

Liu, M., Zhang, Q., Fan, F., Shen, S., 2018. Experiments on natural snow distribution around simplified building models based on open air snow-wind combined experimental facility. J. Wind Eng. Ind. Aerod. 173, 1–13.

Luo, W., Dong, Z., Qian, G., Lu, J., 2012. Wind tunnel simulation of the three-dimensional airflow patterns behind cuboid obstacles at different angles of wind incidence, and their significance for the formation of sand shadows. Geomorphology 139, 258–270.

Malavasi, M., Santoro, R., Cutini, M., Acosta, A.T.R., Carranza, M.L., 2013. What has happened to coastal dunes in the last half century? A multitemporal coastal landscape analysis in Central Italy. Landsc. Urban Plann. 119, 54–63.

Martinuzzi, R., Tropea, C., 1993. The flow around surface-mounted, prismatic obstacles placed in a fully developed channel flow (data bank contribution). J. Fluid Eng. 115 (1), 85–92.

McKenna Neuman, C., Bédard, O., 2015. A wind tunnel study of flow structure adjustment on deformable sand beds containing a surface-mounted obstacle. J. Geophys. Res.: Earth Surf. 120 (9), 1824–1840.

McKenna Neuman, C., Sanderson, R.S., Sutton, S., 2013. Vortex shedding and morphodynamic response of bed surfaces containing non-erodible roughness elements. Geomorphology 198, 45–56.

Morton, R.A., Paine, J.G., Gibeaut, J.C., 1994. Stages and durations of post-storm beach recovery, southeastern Texas coast, USA. J. Coast Res. 10 (4), 884–908.

Nordstrom, K.F., McCluskey, J.M., 1984. Considerations for control of house construction in coastal dunes. Coast. Manag. 12 (4), 385–402.

Nordstrom, K.F., McCluskey, J.M., 1985. The effects of houses and sand fences on the eolian sediment budget at fire island, New York. J. Coast Res. 1 (1), 39–46.

Oikawa, S., Tomabechi, T., 2000. Daily Observation of Snowdrifts Around a Model Cube. Fourth Conference of Snow Engineering, pp. 137–141.

Oke, T.R., Mills, G., Christen, A., Voogt, J.A., 2017. Airflow, Urban Climates. Cambridge University Press, Cambridge, pp. 77–121.

Peterka, J.A., Meroney, R.N., Kothari, K.M., 1985. Wind flow patterns about buildings. J. Wind Eng. Ind. Aerod. 21 (1), 21–38.

Poppema, D.W., 2020. The Effect of Buildings on the Morphological Development of the Beach-Dune System: Literature Report. 2020R-001-WEM-001. University of Twente, Enschede.

Poppema, D.W., Wijnberg, K.M., Mulder, J.P.M., Hulscher, S.J.M.H., 2019. Scale Experiments on Aeolian Deposition and Erosion Patterns Created by Buildings on the Beach, Coastal Sediments 2019. World Scientific, pp. 1693–1707. https://doi.org/10.1142/9789811204487_0146.

Reinders, J., Van der Valk, B., Van der Meulen, F., 2014. Effecten van tijdelijke strandbebouwing op de ontwikkeling van de jonge zeereep (H2130: Wit duin) aan de zeezijde van de duincompensie Delfstandse kust (in Dutch). Deltares, Delft, 1206682-000-zks-0014.

Rotnicka, J., 2013. Aeolian vertical mass flux profiles above dry and moist sandy beach surfaces. Geomorphology 187, 27–37.

Sauvola, J., Pietikäinen, M., 2000. Adaptive document image binarization. Pattern Recogn. 33 (2), 225–236.

Scarelli, F.M., et al., 2017. Seasonal dune and beach monitoring using photogrammetry from uav surveys to apply in the iczm on the ravenna coast (emilia-romagna, Italy). Rem. Sens. Appl.: Soc. Environ. 7, 27–39.

Schulman, L.L., Strimaitis, D.G., Scire, J.S., 2000. Development and evaluation of the prime plume rise and building downwash model. J. Air Waste Manag. Assoc. 50 (3), 378–390.

Senthilkumaran, N., Vaithegi, S., 2016. Image segmentation by using thresholding techniques for medical images. Comput. Sci. Eng.: Int. J. 6 (1), 1–13.

Shafait, F., Keysers, D., Breuel, T.M., 2008. Efficient implementation of local adaptive thresholding techniques using integral images. Document recognition and retrieval XV, 681510.

Smith, A.B., Jackson, D.W.T., Cooper, J.A.G., Hernández-Calvento, L., 2017. Quantifying the role of urbanization on airflow perturbations and dunefield evolution. Earth's Future 5 (5), 520–539.

Sturdivant, E.J., et al., 2017. UAS-SfM for coastal research: geomorphic feature extraction and land cover classification from high-resolution elevation and optical imagery. Rem. Sens. 9 (10), 1020.

Theil, H., 1961. Economic Forecasts and Policy. North-Holland Pub. Co., Amsterdam.

Thiis, T.K., 2003. Large scale studies of development of snowdrifts around buildings. J. Wind Eng. Ind. Aerod. 91 (6), 829–839.

Thiis, T.K., Gjessing, Y., 1999. Large-scale measurements of snowdrifts around flat-roofed and single-pitch-roofed buildings. Cold Reg. Sci. Technol. 30 (1), 175–181.

Tominaga, Y., Okaze, T., Mochida, A., 2018. Wind tunnel experiment and CFD analysis of sand erosion/deposition due to wind around an obstacle. J. Wind Eng. Ind. Aerod. 182, 262–271.

Tsoar, H., 1983. Wind Tunnel Modeling of Echo and Climbing Dunes. In: Brookfield, M. E., Ahlbrandt, T.S. (Eds.), Developments in Sedimentology: Eolian Sediments and Processes. Elsevier, pp. 247–259.

Tsoar, H., Blumberg, D., 1991. The Effect of Sea Cliffs on Inland Encroachment of Aeolian Sand. Aeolian Grain Transport, Vienna, pp. 131–146.

Ungar, J.E., Haff, P.K., 1987. Steady state saltation in air. Sedimentology 34 (2), 289–299.

Van Puijenbroek, M.E.B., et al., 2017. Exploring the contributions of vegetation and dune size to early dune development using unmanned aerial vehicle (UAV) imaging. Biogeosciences 14 (23), 5533–5549.
White, B.R., 1996. Laboratory simulation of aeolian sand transport and physical modeling of flow around dunes. Ann. Arid Zone 35 (3), 187–213.
Wilson, D.J., 1979. Flow patterns over flat roofed buildings and application to exhaust stack design. ASHRAE Trans 85, 284–295.
Winckel, P.R., Vrijling, J.K., Van de Graaff, J., 2008. Developing a building policy for the erosion zone: solutions to some key (Dutch) questions. Coast Eng. 55 (1), 79–92.